Front. Phys., 2012, 7(6): 701–707
DOI 10.1007/s11467-012-0272-x

REVIEW ARTICLE

Detection of explosives with laser-induced breakdown spectroscopy

Qian-Qian Wang†, **Kai Liu**, **Hua Zhao**, **Cong-Hui Ge**, **Zhi-Wen Huang**

School of Optoelectronics, Beijing Institute of Technology, Beijing 100081, China

E-mail: † *qqwang@bit.edu.cn*

Received May 30, 2012; accepted September 27, 2012

Our recent work on the detection of explosives by laser-induced breakdown spectroscopy (LIBS) is reviewed in this paper. We have studied the physical mechanism of laser-induced plasma of an organic explosive, TNT. The LIBS spectra of TNT under single-photon excitation are simulated using MATLAB. The variations of the atomic emission lines intensities of carbon, hydrogen, oxygen, and nitrogen versus the plasma temperature are simulated too. We also investigate the time-resolved LIBS spectra of a common inorganic explosive, black powder, in two kinds of surrounding atmospheres, air and argon, and find that the maximum value of the O atomic emission line SBR of black powder occurs at a gate delay of 596 ns. Another focus of our work is on using chemometic methods such as principle component analysis (PCA) and partial least squares discriminant analysis (PLS-DA) to distinguish the organic explosives from organic materials such as plastics. A PLS-DA model for classification is built. TNT and seven types of plastics are chosen as samples to test the model. The experimental results demonstrate that LIBS coupled with the chemometric techniques has the capacity to discriminate organic explosive from plastics.

Keywords laser-induced breakdown spectroscopy (LIBS), Raman spectroscopy, principle component analysis (PCA), partial least squares discriminant analysis (PLS-DA), explosive

PACS numbers 42.62.Fi, 52.50.Jm, 42.62.-b

Contents

1 Introduction

Explosives detection can be divided into detection of bulk explosives and detection of trace amounts of explosives [1]. Common techniques for detection of bulk explosives include the X-ray analysis, neutron activation or scattering and other imaging methods based on nuclear technology [2]. Most widely accepted techniques for detection of traces of explosives are ion-mobility spectrometry (IMS) and gas chromatography [3–5]. Both of them rely on vapor detection. When the vapor concentrations of explosives are very small for example at the room temperatures and specially in good sealing condition [6], it is hard to detect using IMS and gas chromatography. In addition, these techniques cannot achieve real-time and standoff detection either. Therefore, it is urgent to find a true standoff method for detection of explosive residues.

Laser-induced breakdown spectroscopy (LIBS) is an optical spectroscopic technique which can determine the elemental composition from the light emission of laser-generated plasma on the basis of elemental and molecular emission intensities. Due to its unique advantages such as no sample preparation, high sensitivity, real-time detection, LIBS has been widely used for numerous applications [7–13]. Recently more and more research teams have begun to research about using LIBS to detect explosives [10, 14–17] because LIBS is a suitable technique for standoff detection and analysis [18].

We have been carrying on three aspects of research about LIBS for explosives detection: simulating LIBS spectra of explosives, detecting LIBS spectra of explosives, and analyzing LIBS spectra of explosives using chemometric approaches such as principal component analysis (PCA)and partial least square method (PLS).

2 Modeling of LIBS emission lines of TNT

The aim of our work is to develop a model of the LIBS emission lines of trinitrotoluene (TNT). We choose TNT as the sample because it is widely used in military and industrial applications. According to the literatures, the laser ablation process is mainly based on two mechanisms: photothermal and photochemical ablations. The former process is dominant in ablation processes with long wavelength such as infrared laser pulse, where rapid thermalization happens and decomposition of heated material occurs following the Arrhenius law. The second process occurs in ablation with short wavelength such as ultraviolet laser pulse, where direct bond breaking happens due to the excitation of an incoming laser pulse.

As the first step, we assume that each chemical bond of TNT is broken by one incident photon and the atom generated by bond breaking is stimulated to an excited electronic state with higher energy by absorbing energy of one incident photon. This excitation process can be expressed as

$$A + h\nu \rightarrow A^* \tag{1}$$

where $h\nu$ is the energy of one photon. The excited atoms will come back to ground state or an excited state with lower energy normally in 10^{-8} s and emit radiation with particular wavelengths.

Laser-induced plasma can be considered in local thermodynamic equilibrium situation, with the atom population following Boltzmann distribution law. The atom population at excited state with energy level m is

$$N_m = \frac{g_m}{G} N \exp\left(-\frac{E_m}{KT}\right) \tag{2}$$

where N_m is the atom population at energy level m; g_m is the degeneracy of the energy level m; E_m is the energy of the excited state m; K is Boltzmann constant; T is temperature; G is the partition function which can be expressed as

$$G = \sum_{i=0}^{m} g_i \exp\left(-\frac{E_i}{KT}\right) \tag{3}$$

When we ignored the stimulated emission and self-absorption effect, the intensity of the emission line is

$$I_{mn} = A_{mn} h\nu_{mn} \frac{g_m}{G} N \exp\left(-\frac{E_m}{KT}\right) \tag{4}$$

where A_{mn} is the transition probability of spontaneous radiation. If we know the value of all the parameters in Eq. (4), the intensity of the emission line can be calculated.

Based on the analysis above, we developed a model of one-photon absorption to simulate the emission lines of TNT laser-induced plasma. TNT consists of four elements: carbon, hydrogen, nitrogen, and oxygen. Its molecular structure is shown in Fig. 1. Energies of mol bonds and single-molecule bonds in TNT are listed in Table 1.

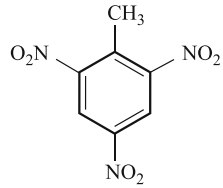

Fig. 1 Molecular structure of TNT.

Table 1 Energies of mol bonds and single-molecule bonds in TNT.

Bond	C–H	C–C	C=C	C–N	N=O
Mol bond energy /(kal·mol^{-1})	413	348	614	305	607
Single-molecule bond energy /eV	4.29	3.61	6.37	3.17	6.30

The decomposition process of the molecular with the increase of incident photon energy is shown in Fig. 2. The C–N bond is broken first, and then C–C, C–H, and N=O are broken sequentially with the increase of incident photons energy.

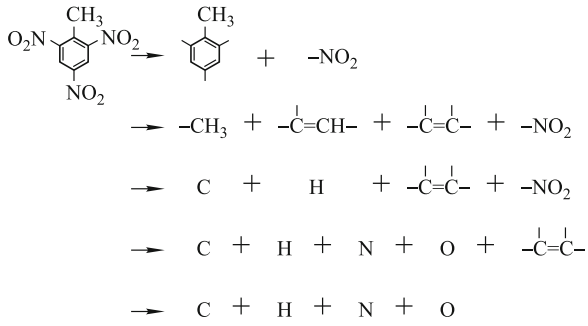

Fig. 2 Decomposition process of TNT molecular with the increase of photon energy.

If the energy of incident photons is strong enough, in this case the photon energy $h\nu > 12.124\ 79$ eV and the corresponding photon wavelength $\lambda < 102.5$ nm, the TNT molecular will be decomposed into C, H, O, and N atoms. These atoms absorb the incident photons energy and transfer to excited states with higher level energy. When they come back to ground state or an excited state with lower energy, they will emit radiation with particular wavelengths. We assume that the incident photon's wavelength is 102 nm and the temperature in the plasma is 10 000°C, the emission lines simulated by MATLAB are shown in Fig. 3.

Figure 3 shows all emission lines of electronically excited carbon, hydrogen, nitrogen, and oxygen atoms. It can be seen from Fig. 3(a) that carbon lines are at 156.2 nm, 165.7 nm, 193 nm and 247.9 nm, and the intensities of lines at 165.7 nm and 193 nm are much stronger than the other lines. Figure 3(b) shows that the hydrogen lines at 102.5 nm and 121.6 nm are much stronger than the line at 656 nm. As shown in Fig. 3(c), an oxygen

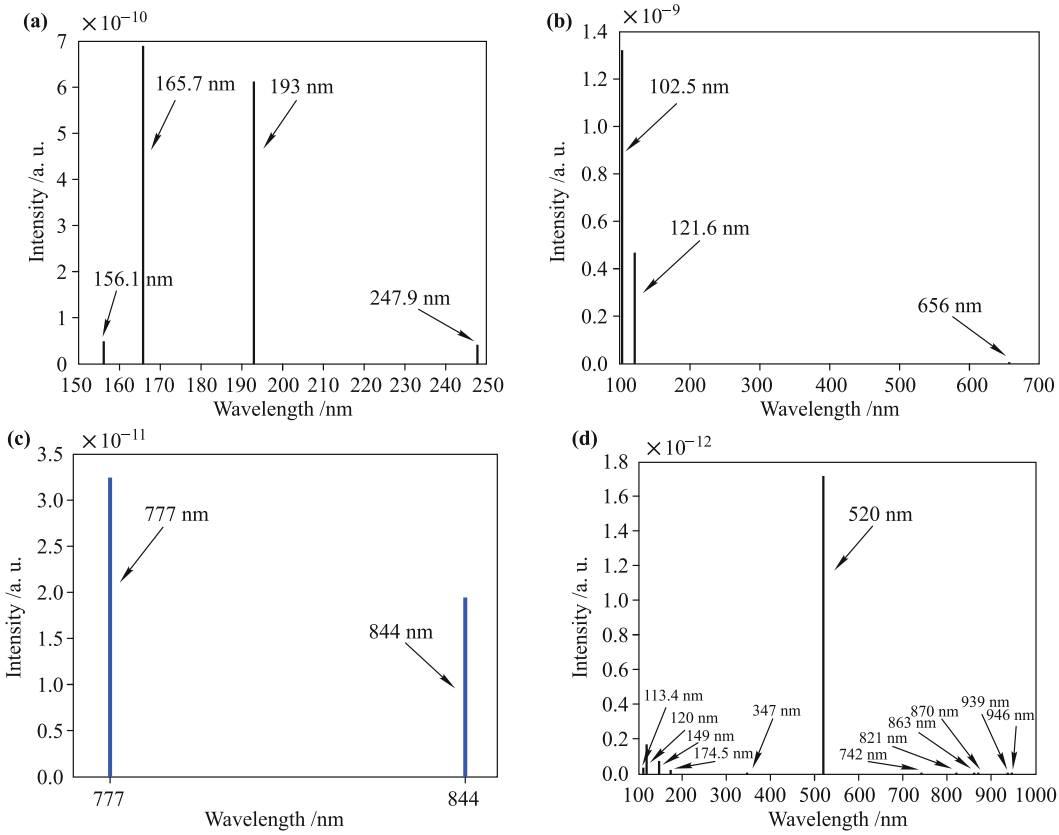

Fig. 3 Simulated LIBS emission spectra of carbon **(a)**, hydrogen **(b)**, oxygen **(c)**, and nitrogen **(d)** atoms.

atom has two strong lines at 777 nm and 844 nm. We can see from Fig. 3(d) that the strongest line of nitrogen is at 520 nm and the other 11 lines are too weak to see.

We also simulate the variation of line intensity versus plasma temperature. The wavelength of incident photon is still set as 102 nm. The range of plasma temperature is set from 8000 K to 20 000 K according to the experimental results. The variation of the intensities of carbon 165.7 nm and 193 nm lines versus the plasma temperature are shown in Fig. 4.

From Fig. 4 it can be seen that different lines have different intensity variation versus plasma temperature. The intensity of the carbon line at 165.7 nm decreases with the plasma temperature. However, the intensity of the carbon line at 193 nm increases with the temperature. The reason is that the increasing rates of partition function G and $\exp(-E_m/(KT))$ with the temperature are different for different lines. According to Eqs. (3) and (4), both G and $\exp(-E_m/(KT))$ increase with the temperature. If the increasing rate of G is bigger than that of $\exp(-E_m/(KT))$, the intensity of the atomic emission line will decrease with the temperature. Otherwise, the line intensity will increase with the temperature. The same simulation results can be obtained for hydrogen,

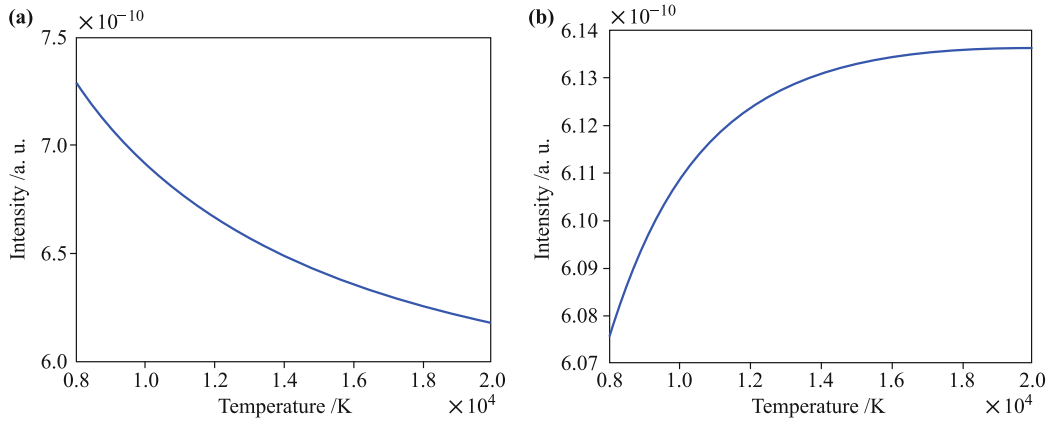

Fig. 4 Variation of intensity of the carbon lines at 165.7 nm **(a)** and 193 nm **(b)** versus the plasma temperature.

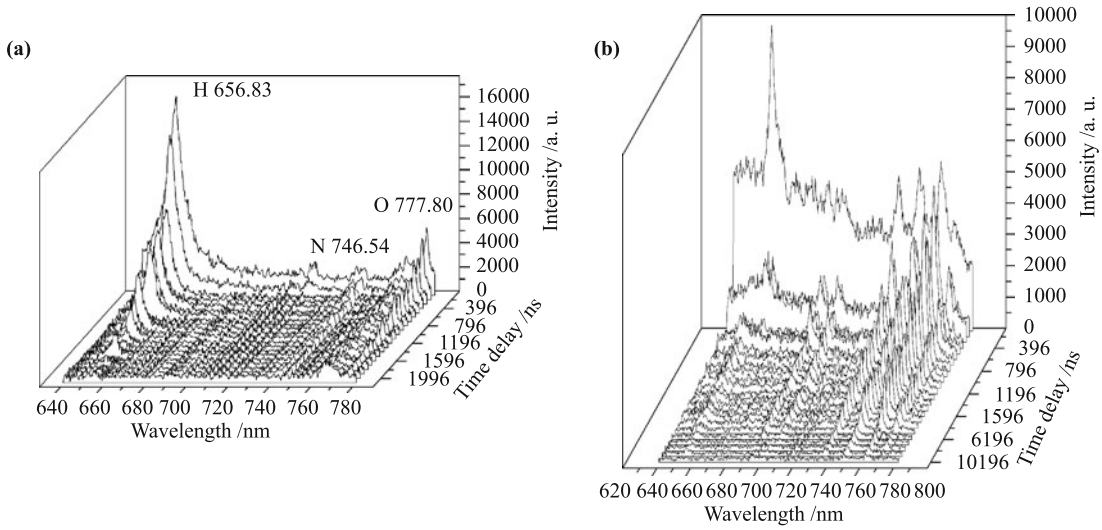

Fig. 5 LIBS emission spectra of black powder in air **(a)** and under argon **(b)** at various gate delay times 96–2096 ns, 96–10 196 ns, respectively.

oxygen and nitrogen atoms.

3 LIBS detection of inorganic explosive

We have investigated the LIBS spectrum of a common inorganic explosive, black powder [19]. For this experiment, an actively Q-switched Nd:YAG laser with 1 064 nm wavelength, 16 ns pulse width, about 130 mJ pulse energy was chosen as the excitation source. The spectrometer was a Czerny–Turner spectrometer (Model MS257 from ORIEL Inc.) with 2 mm slit width, 1200 L/mm grating, around 140 nm spectral width. To detect the emission line of hydrogen, nitrogen, and oxygen, the spectral range was set from 640 nm to 782 nm. The detector was a semiconductor-cooled intensified charge-coupled device (ICCD) (Andor Chip, Model EEV02-06). The integration time gate width of the ICCD detector was fixed at 100 ns. A pulse delayer (DG535 from Stanford Research Systems, Inc.) was used to control the gate delay time.

We choose black powder and one of its key components, KNO_3, as samples. Meanwhile, $NaNO_3$ is chosen as the reference, because it is similar to KNO_3. Both of them are white powder. The LIBS spectra of black powder in air and under argon at various gate delay times are shown in Fig. 5.

It can be seen from Fig. 5 that both the peak intensities of lines and the intensity of background decline with an increasing gate delay time. The decay ratios of peak intensities under argon are slower than those in air. The atomic emission intensities of black powder (hydrogen, nitrogen, and oxygen) decline to the same level as the background intensity in air when the gate delay is beyond 1396 ns. However, under argon the value is 5096 ns.

The signal-to-background ratio (SBR) of the atomic emission intensity of oxygen is used to determine the optimal timing. The SBR of the O atomic emission line at 777 nm of $NaNO_3$, KNO_3, and black powder at various gate delay times are shown in Fig. 6. The maximal SBR value occurs at a gate delay of 596 ns.

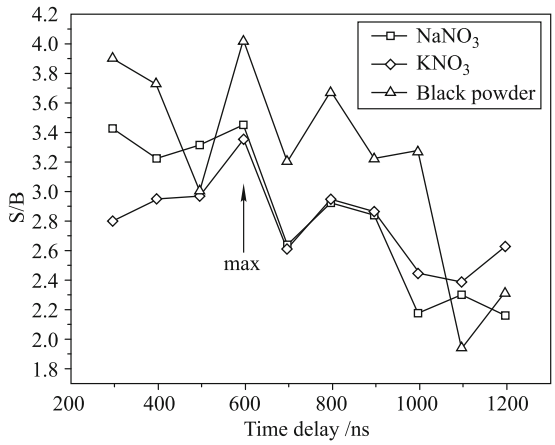

Fig. 6 The SBR of O atomic emission lines of black powder, $NaNO_3$ and KNO_3 versus gate delay from 296 ns to 1196 ns in air.

The LIBS spectra of black powder, KNO_3, and $NaNO_3$ at a gate delay of 596 ns in air and under argon are shown in Fig. 7. It can be seen that there is almost no hydrogen line in LIBS spectra of black powder and $NaNO_3$ under argon. And the intensities of nitrogen and oxygen lines are also smaller than those in air. It shows that the intensities of hydrogen, nitrogen, and oxygen lines mainly come from surrounding air. To get real LIBS spectra of samples, we must try to eliminate the influence from ambient air.

We can see a clear potassium emission line at 766.31 nm in Fig. 7(b). The intensity of kalium line is much stronger under argon than in air due to the increase of the amplification factor of ICCD. For some unknown

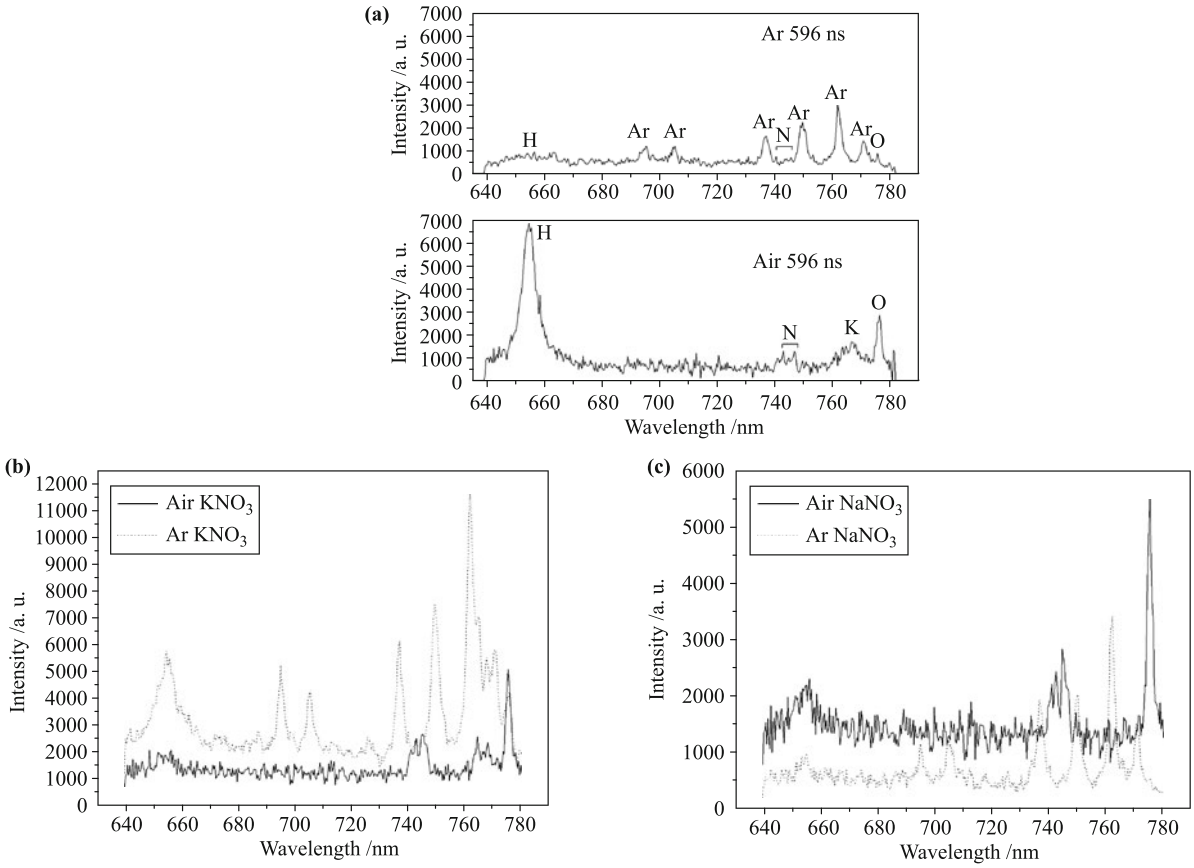

Fig. 7 LIBS spectra of **(a)** black powder, **(b)** KNO_3, and **(c)** $NaNO_3$ in two different kinds of surrounding atmosphere at time delay of 596 ns.

reasons there is a strong hydrogen line in the spectrum of KNO_3 under argon. There is no sodium emission line in Fig. 7(c), because the spectral detection range is from 640 nm to 782 nm and Na lines are around 589 nm.

4 Multivariate analysis of LIBS

The coupling of LIBS with multivariate analysis has been used for numerous applications [20]. The focus of our work is on how to use principal component analysis (PCA) and partial least squares discriminant analysis (PLS-DA) to distinguish an organic explosive, TNT, from plastics [21]. We choose seven kinds of plastics as samples: acrylonitrile butadiene styrene (ABS), high density polyethylene (HDPE), polyethylene terephthalate (PET), polymethyl methacrylate (PMMA), polypropylene (PP), polystyrene (PS), and polyvinyl chloride (PVC). The LIBS emission spectra of these samples were collected by an Echelle spectrometer (of about 10 pm average resolution, 200–838 nm spectral range) with an ICCD detector (with delay time of 200 ns, gate width of 10 ms). The excitation source was a frequency-quadrupled Q-switch Nd:YAG laser (New Wave Tempest-20, 266 nm wavelength, 20 Hz repetition rate, 4 ns pulse width). All of the multivariate analysis was performed using Statistica version 8.0 (Statsoft, Inc.).

A PCA model is constructed based on intensities of 21 emission lines from the LIBS spectra of 200 samples for each kind of plastic and 231 samples of TNT. The scores of the first two PCs of the TNT and plastic samples are plotted in Fig. 8. The separation between TNT and plastics is easily distinguishable. The PP samples are closest to the TNT, and there is one PP sample mixed with TNT samples. Most of the TNT samples cluster together. However, two TNT samples are far away from the others for some unknown reasons. The separation between each kind of plastics is not established. Among

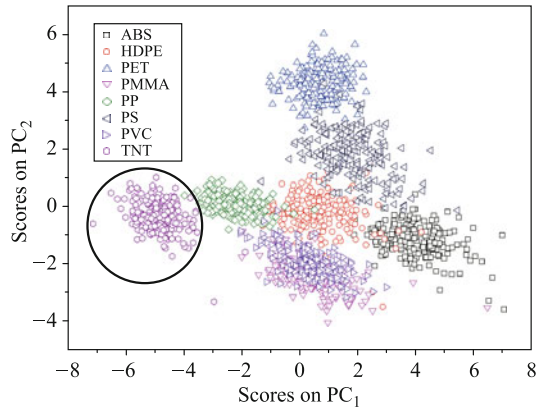

Fig. 8 The scores of the first two PCs of the TNT and plastic samples.

them, PET, PP, and PS samples can be basically separated from each other. There is more overlap between these samples. PMMA, ABS, HDPE, and PVC samples are totally overlapped with each other, although their LIBS spectra look very different.

We use a receiver operating characteristic (ROC) curve, as shown in Fig. 9, to test the performance of this PCA model. The area below ROC curve is beyond 0.99, which means that the PCA model has perfect discrimination of TNT and plastics.

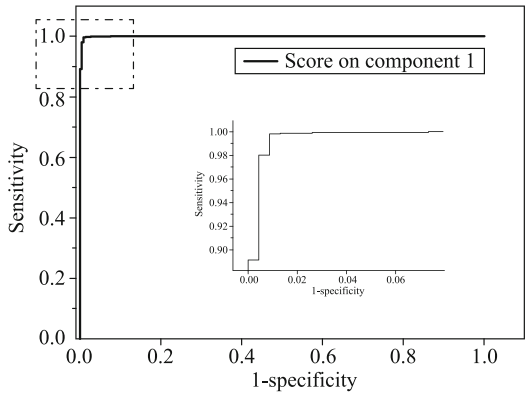

Fig. 9 The ROC curve generated for the PCA model.

In the case of PLS-DA analysis, two input matrices, $\boldsymbol{X}$ and $\boldsymbol{Y}$, are used to describe the materials to be classified. The $\boldsymbol{X}$ matrix contains the atomic line intensities of each individual spectrum. The $\boldsymbol{Y}$ matrix contains the class information. For PLS-DA model building, the intensities of 21 emission lines from 100 PVC, 100 PS, 100 PP, 100 PMMA, 100 PET, 100 HDPE, 100 ABS, and 100 TNT LIBS spectra are entered into the $\boldsymbol{X}$ matrix. The $\boldsymbol{Y}$ matrix contains the classification of each sample. Plastics and TNT spectra are labeled class 0 and 1, respectively. $\boldsymbol{X}$ and $\boldsymbol{Y}$ matrices are imported into the software Statistica 8.0 to build the PLS discriminant model for these eight kinds of samples. Figure 10 shows the PLS discriminant analysis results. The y-axis represents the class prediction. The x-axis is simply a sample index. It can be seen that TNT samples are separated clearly from plastics samples.

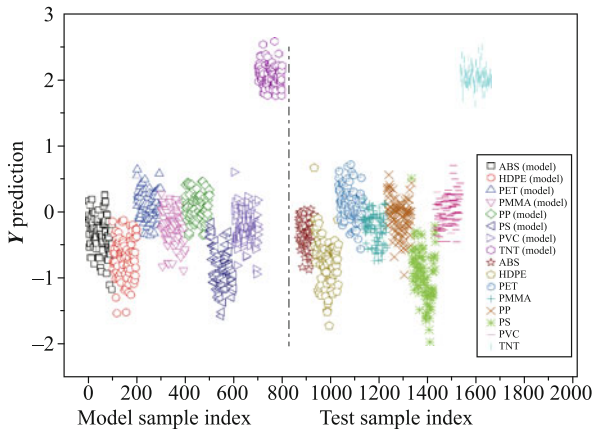

Fig. 10 PLS-DA plot of test samples against PLS-DA model that includes TNT and seven types of plastics.

800 "unknown" spectra (100 spectra from each type of samples) not used in building the model are used as a test set to test the performance of the PLS-DA model. The prediction results are also shown in Fig. 10. All 100 of the TNT spectra are above 1, and therefore are correctly classified as explosives. The other 700 samples are all below 1 and are correctly classified as non-explosives. Excellent separation between explosives and non-explosives is achieved for this model and test set. These results show that the discrimination between TNT and plastics is possible using LIBS and multivariate analysis, although they have similar atomic composition.

5 Conclusions

We have simulated the LIBS emission spectra of TNT under single-photon excitation and the variations of the atomic emission line intensities of carbon, hydrogen, oxygen, and nitrogen versus the plasma temperature. However, in real-life situations multi-photon excitation also exists. As a result, for future work we also need to simulate the LIBS spectra under multi-photon excitation and try to demonstrate the correctness of simulation by experimental results.

We have investigated the time-resolved LIBS spectra of a common inorganic explosive, black powder, in air and under argon and find the optimal value of the signal-to-background ratio of oxygen emission line at a delay of 596 ns. The experimental results demonstrate that an argon flow can be used to displace air to eliminate the oxygen and nitrogen contribution from air for sensitive and selective LIBS detection of explosives.

We have shown that PCA and PLS-DA are able to discriminate among the sample spectra of organic explosives and plastics. In the next step we will apply spectra acquired under different conditions to our model. We will also investigate whether the model is good enough for discriminating explosives from all other materials.

Acknowledgements This work has been carried out with a financial grant from the National Natural Science Foundation of China (Grant No. 60978035). The authors would like to thank Fraunhofer Institute of Laser Technology in Germany for providing some experimental equipments and TNT samples.

References

1. C. Pasquini, J. Cortez, L. M. C. Silva, and F. B. Gonzaga, J. Braz. Chem. Soc., 2007, 18(3): 463
2. J. E. Parmeter, in: 38th Annual International Carnahan Conference on Security Technology, IEEE, Albuquerque, NM, 2004: 355
3. T. L. Buxton and P. B. Harrington, Appl. Spectrosc., 2003,

57(2): 223

4. O. L. Collin, C. M. Zimmermann, and G. P. Jackson, Int. J. Mass Spectrom., 2009, 279(2–3): 93
5. G. W. Cook, P. T. LaPuma, G. L. Hook, and B. A. Eckenrode, J. Forensic Sci., 2010, 55(6): 1582
6. J. I. Steinfeld and J. Wormhoudt, Annu. Rev. Phys. Chem., 1998, 49(1): 203
7. A. P. M. Michel, Spectrochim. Acta B, 2010, 65: 185
8. J. S. Huang, Q. L. Chen, and W. D. Zhao, Spectrosc. Spect. Anal., 2009, 29: 3126
9. D. Q. Yuan and J. T. Xu, Adv. Mater. Res., 2011, 179–180: 1183
10. P. Lucena, A. Dona, L. M. Tobaria, and J. J. Laserna, Spectrochim Acta B, 2011, 66(1): 12
11. V. K. Singh, A. K. Rai, P. K. Rai, and P. K. Jindal, Lasers Med. Sci., 2009, 24(5): 749
12. Z. X. Lin, L. Chang, J. Li, and L. M. Liu, Spectrosc. Spect. Anal., 2009, 29: 1675
13. K. Liu, Q. Q. Wang, H. Zhao, and Y. L. Xiao, Spectrosc. Spect. Anal., 2011, 31: 1171
14. S. Sreedhar, M. A. Kumar, G. M. Kumar, P. P. Kiran, S. P. Tewari, and S. V. Rao, 2010, Proc. SPIE 7665 Chemical Biological, Radiological, Nuclear, and Explosives (CBRNE) Sensing XI (Orlando, Florida, USA, 6–8 April, 2010: 76650T
15. J. Handke, F. Duschek, K. Grunewald, and C. Pargmann, 2011, Proc. SPIE 8018 Chemical, Biological, Radiological, Nuclear, and Explosives (CBRNE) Sensing XII (Orlando, Florida, USA, 26–28 April, 2011: 80180T
16. V. Lazic, A. Palucci, S. Jovicevic, C. Poggi, and E. Buono, Spectrochim. Acta B, 2009, 64: 1028
17. Q. Q. Wang, P. Jander, C. Fricke-Begemann, and R. Noll, Spectrochim. Acta B, 2008, 63: 1011
18. J. L. Gottfried, C. A. De Lucia, Munson, and A. W. Miziolek, Anal. Bioanal. Chem., 2009, 395(2): 283
19. H. Zhao, Q. Q. Wang, K. Liu, and C. H. Ge, Spectrosc. Spect. Anal., 2012, 32: 577
20. J. L. Gottfried, R. S. Harmon, F. C. De Lucia, and A. W. Miziolek, Spectrochim. Acta B, 2009, 64: 1009
21. D. L. Death, A. P. Cunningham, and L. J. Pollard, Spectrochim. Acta B, 2009, 64: 1048
22. B. L. Sun, J. L. Liu, and Y. B. Cai, Spectrosc. Spect. Anal., 2011, 31: 366
23. T. Galeano-Diaz, M. I. Acedo-Valenzuela, N. Mora-Diez, and A. Silva-Rodriguez, Electroanal., 2011, 23(2): 449
24. J. L. Jr De Lucia, C. A. Gottfried, Munson, and A. W. Miziolek, Appl. Opt., 2008, 47(31): G112
25. Q. Q. Wang, K. Liu, and H. Zhao, Chin. Phys. Lett., 2012, 29(4): 044206